PCCP

Accepted Manuscript

ROYAL SOCIETY OF CHEMISTRY

www.rsc.org/pccp

Nematic ordering of polarizable colloidal rods in an external electric field: theory and experiment

Thomas Troppenz[1], Anke Kuijk[2], Arnout Imhof[2], Alfons van Blaaderen[2], Marjolein Dijkstra[2], and René van Roij[1]

[1] *Institute for Theoretical Physics, Center for Extreme Matter and Emergent Phenomena, Utrecht University, Leuvenlaan 4, 3584 CE Utrecht, the Netherlands*

[2] *Soft Condensed Matter, Debye Institute for Nanomaterials Science, Utrecht University, Princetonplein 5, 3584 CC Utrecht, the Netherlands.*

We employ the coupled dipole method [B. W. Kwaadgras et. al., J. Chem. Phys. **135**, 134105 (2011)] to calculate the orientation-dependent interaction of polarizable colloidal rods with an external electric field. We project the angular distribution function of a system of such rods on a quasi-two-dimensional slab, corresponding to the focal plane of a microscope, and show that the $3D$ nematic order parameter and its measurable projected analogue are very similar. We compare our results to confocal microscopy measurements on the orientation distribution function of systems of polarizable colloidal silica rods in an external electric field, demonstrating reasonably good agreement between theory and experiment without any free fit parameter.

INTRODUCTION

The self-assembly of Brownian nanoparticles received much attention in recent years, which is to a large extent due to their ability to form ordered structures. This is of great interest for materials science, since these nanostructures may yield new applications.

Electric fields can be used to control the orientation and relative position of anisotropic polarizable colloidal particles [1–11], which is of great practical interest, since it creates the possibility of influencing and directing the self-assembly process of such systems. This practical potential is demonstrated by applications such as e-paper [12] and liquid-crystal displays [13]. Recently, great progress has been made in the synthesis of anisotropic colloidal particles, such as rod-like particles [14–16], dimer particles [10, 11, 17–24] and bowl-shaped particles [25–31]. For such anisotropic particles, the coupled dipole method (cdm) has been employed successfully to calculate properties such as the polarizability tensor [8, 32], the orientation-dependent energy [8, 9], and the electric-field induced dipole interactions [33]. This has been done for many different particle shapes, including needles, bowls, dumbbells, cuboids [8] and many others. Here, we use a similar theoretical framework to calculate the orientation-dependent energy of a polarizable colloidal rod in a high-dielectric solvent subject to an external electric field, and from this its thermal orientation distribution function. We then proceed to compare the theoretical predictions to experimental confocal microscopy measurements in dilute systems using a novel experimental model system of colloidal silica rods of varying length L and diameter D.

Confocal microscopy [34] is an important experimental tool to quantitatively visualize the self-assembly process or the resulting self-assembled structure using three-dimensional (3D) data sets, which are built up from stacks of 2D slices. 3D position coordinates for spherical particles [34], and for rod-like particles also the orientation [35], can be obtained from such data sets. However, if the dynamics of the individual particles is too fast compared to the time it takes to obtain such 3D stacks, as is the case with the rod-like particles studied in this paper, this 3D construction process from many 2D slices is not possible. One way to still follow the dynamics or a self-assembly process under these conditions is to acquire 2D slices as quickly as possible. An important complication that manifests itself in this case in confocal measurements of anisotropic particles is that only the *projection* of each particle onto the focal plane, as determined by the width of the point spread function along the optical axis [34], is observable. This not only leads to an apparent polydispersity because different orientations of identical particles lead to different projection shapes, but it also leads to an orientation dependent detection efficiency since particles with their center of mass outside the plane may get detected anyway if a "tip" resides inside the focal plane. In this paper we address these projection and detection issues for the case of homogeneously fluorescently labeled micron-sized cylindrical rods aligned by an external electric field. Interestingly, and perhaps surprisingly, we will show that reliable information on the full (unprojected) orientation distribution can be obtained from measurements of the projected orientations.

Below we develop a method to compare the measured orientation distribution function in an essentially two-dimensional confocal slab of finite thickness Δ to the fully $3D$-resolved distribution $\Psi(\theta)$ that follows directly from our theory with θ the angle between the applied electric field and the long axis of a rod. We find rather good agreement between theory and experiment, without any free fit parameter. In addition, we will also show that the nematic order parameter obtained from rod-orientations projected onto the focal plane agree remarkably well with the nematic order parameter based on the fully 3D (unprojected) orientations of the rods. This finding is also relevant for the interpretation of confocal microscopy ob-

servations of other anisotropic particles that move too quickly with respect to the time it takes to acquire 3D data sets.

CDM OF A POLARIZABLE PARTICLE IN A SOLVENT

We consider a single rod of dielectric constant ϵ_1 in a solvent of dielectric constant ϵ_2 in a homogeneous and static external electric field $\mathbf{E}$ that polarizes both the solvent and the rod as illustrated in Fig. 1. We describe

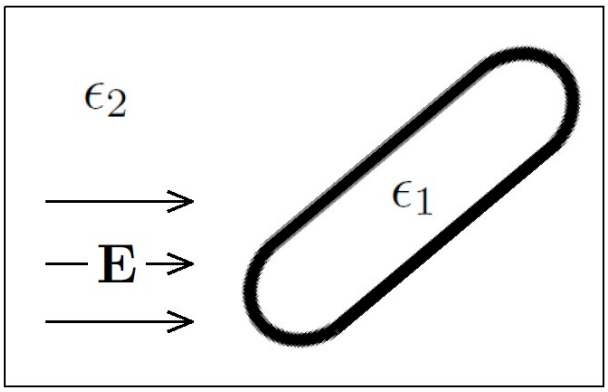

Figure 1. Sketch of a colloidal rod of dielectric constant ϵ_1 in a solvent of dielectric constant ϵ_2 exposed to a homogeneous external electric field $\mathbf{E}$.

the dielectric rod in terms of polarizable units that we call atoms for simplicity. The atoms are located on a fixed cubic grid of N lattice sites $\mathbf{r}_i$ with $1 \leq i \leq N$ such that they build up the rod. They are modeled as Lorentz-atoms with a dipole moment $\mathbf{p}_i = e\mathbf{u}_i$, with e the effective electron charge and $\mathbf{u}_i$ the displacement of the effective electron cloud with respect to $\mathbf{r}_i$ [8]. The atom's polarization $\mathbf{p}_i$ is linearly dependent on the local electric field $\mathbf{E}^{(i)}_{loc}$ that atom i is subjected to, so

$$\mathbf{p}_i = \alpha \mathbf{E}^{(i)}_{loc}. \tag{1}$$

Here, α is the molecular excess polarizability given by the Clausius-Mossotti relation

$$\alpha = \frac{3}{4\pi}\frac{\epsilon_2}{n_0}\frac{\epsilon_1 - \epsilon_2}{\epsilon_1 + 2\epsilon_2}, \tag{2}$$

where n_0 denotes the number density of the dipoles in the rod. We note that the Clausius-Mossotti relation may lead to negative as well as positive values for α. It is important to note that $\mathbf{p}_i$ and $\mathbf{u}_i$ are anti-parallel to $\mathbf{E}^{(i)}_{loc}$ when $\alpha < 0$. In other words, the physics for $\alpha > 0$ is not identical to that of $\alpha < 0$ because the induced electric field due to neighboring atoms is to be added to or subtracted from the applied electric field, as will be made explicit below.

The Lorentz atoms couple to the external electric field $\mathbf{E}$ by an energy $-e\mathbf{u}_i \cdot \mathbf{E}$ and to each other through a pair potential $-e^2\mathbf{u}_i \cdot \mathbf{T}(\mathbf{r}_i - \mathbf{r}_j) \cdot \mathbf{u}_j$, where i and j represent atoms separated by a spatial distance $\mathbf{r}_i - \mathbf{r}_j$ and where the dipole tensor is given by

$$\mathbf{T}(\mathbf{r}) = \begin{cases} \dfrac{3\hat{\mathbf{r}}\hat{\mathbf{r}} - \mathbf{I}}{\epsilon_2 |\mathbf{r}|^3}, & \text{if } \mathbf{r} \neq \mathbf{0}; \\ \mathbf{0}, & \text{if } \mathbf{r} = \mathbf{0}, \end{cases} \tag{3}$$

with $\hat{\mathbf{r}} = \mathbf{r}/|\mathbf{r}|$ a unit vector, $\mathbf{I}$ the 3×3 identity matrix, and $\mathbf{0}$ the corresponding null matrix.

Note that a dipole at position $\mathbf{r}_j$ generates an electric field at position $\mathbf{r}_i$ given by $\mathbf{T}_{ij} \cdot \mathbf{p}_j$ such that the local electric field can be written as

$$\mathbf{E}^{(i)}_{loc} = \mathbf{E} + \sum_j \mathbf{T}_{ij} \cdot \mathbf{p}_j, \tag{4}$$

where $\mathbf{E}$ is the external electric field as introduced above and $\mathbf{T}_{ij}$ is short for $\mathbf{T}(\mathbf{r}_i - \mathbf{r}_j)$.

Combining Eq. (1) with Eq. (4), we find

$$\mathbf{p}_i = \alpha \mathbf{E} + \alpha \sum_j \mathbf{T}_{ij} \cdot \mathbf{p}_j, \tag{5}$$

which we rewrite in matrix form as

$$(\mathcal{I} - \alpha \mathcal{T}) \cdot \mathcal{P} = \alpha \mathcal{E}. \tag{6}$$

Here, $\mathcal{P}$ is a vector with $3N$ entries containing the N dipole moment vectors $\mathbf{p}_i$, while $\mathcal{E}$ contains N copies of the external electric field $\mathbf{E}$. We also introduced the $3N \times 3N$ unity matrix $\mathcal{I}$ and the $3N \times 3N$ matrix $\mathcal{T}$, which has entries that are given by the $\mathbf{T}_{ij}$. Eq. (6) is a $3N \times 3N$ linear algebra problem for the dipoles $\mathbf{p}_i$ that can be solved numerically with standard methods. The potential energy $\mathcal{V}_E$ is the energy of N induced dipoles given by [1, 8]

$$\mathcal{V}_E = -\frac{1}{2}\sum_{i=1}^{N} \mathbf{p}_i \cdot \mathbf{E} = -\frac{1}{2}\mathbf{E} \cdot \boldsymbol{\alpha}_c \cdot \mathbf{E}, \tag{7}$$

where the 3×3 excess polarizability tensor $\boldsymbol{\alpha}_c$ of the rod is defined by

$$\sum_i \mathbf{p}_i = \boldsymbol{\alpha}_c \cdot \mathbf{E}, \tag{8}$$

such that

$$\boldsymbol{\alpha}_c = \alpha \sum_{i,j} \mathbf{D}_{ij}, \tag{9}$$

with $\mathbf{D}_{ij}$ given by the 3×3 dimensional sub blocks of the $3N \times 3N$ matrix $(\mathcal{I} - \alpha\mathcal{T})^{-1}$ [8]. For a uniaxial rod-like

particle, $\boldsymbol{\alpha}_c$ can be diagonalized with only two independent entries, denoted by $\alpha_{c,\parallel}$ and $\alpha_{c,\perp}$. We then find that the orientation-dependent excess potential energy $\mathcal{V}_E$ takes a particularly simple form [8],

$$\begin{aligned}\mathcal{V}_E(\theta) &= -\frac{1}{2}\left(\alpha_{c,\parallel}-\alpha_{c,\perp}\right)|\mathbf{E}|^2\cos^2\theta + \text{const} \\ &= -\frac{1}{2}N\alpha(f_\parallel - f_\perp)|\mathbf{E}|^2\cos^2\theta + \text{const}, \qquad (10)\end{aligned}$$

where we used the angle $\theta \in [0,\pi/2]$ between the symmetry axis of the rod and the electric field. We introduce the so-called anisotropy factor $\left(f_\parallel - f_\perp\right)$, which is a dimensionless measure for the eigenvalue difference of the eigenvectors of $\boldsymbol{\alpha}_c$ parallel and perpendicular to $\mathbf{E}$, with $f_\parallel = \alpha_{c,\parallel}/N\alpha$, and $f_\perp = \alpha_{c,\perp}/N\alpha$.

In order to solve Eq. (6) for $\mathcal{P}$, we have to ensure that all eigenvalues of $(\mathcal{I}-\alpha\mathcal{T})$ remain positive. Fig. 2(a) shows λ_{min}, the smallest eigenvalue of $(\mathcal{I}-\alpha\mathcal{T})$, as a function of α/a^3, for three different lattice spacings a, for a spherocylinder of length-to-diameter ratio 2.4. We see that the absolute value of α/a^3 must not be too large, otherwise the coupled dipole method breaks down, a phenomenon known as the polarization catastrophe. This catastrophe is due to an unphysically diverging polarisation, where the linear response relation of Eq. (1) breaks down [32]. To avoid this, we must choose α such that $-0.12 \lesssim \alpha/a^3 \lesssim 0.19$, where we note that the lower bound is close to our experimental system of silica rods in a solvent mixture of water and dimethylsulfoxide (see below). We repeated these calculations for spheres and for spherocylinders with $L/D = 5$, and found that this range for α also holds in those cases. We also see from Fig. 2(a) that λ_{min} decreases as we decrease the lattice constant (and hence increase the number N of dipoles that build up the rod). This effect is more pronounced for negative values of the polarizability than for positive ones. It appears from Fig. 2(b), however, that the anisotropy factor $\left(f_\parallel - f_\perp\right)$ is not strongly dependent on the value of the lattice constant a/D used. For comparison, we also plot the anisotropy factor using the decoupled dipole method (ddm), i.e., a grid with dipoles of equal magnitude and direction $\mathbf{p}_i = \alpha\mathbf{E}$, yielding a potential energy of

$$V^{ddm}(\theta) = -\frac{\alpha^2|\mathbf{E}|^2}{2}\sum_{i\neq j}\frac{3\cos^2\theta_{i,j}-1}{r_{ij}^3} + \text{const}, \qquad (11)$$

where $\theta_{i,j}$ denotes the angle between $\mathbf{r}_{ij}$ and $\mathbf{E}$, with $\mathbf{r}_{ij}$ the vector between dipoles i and j, and $r_{ij} = |\mathbf{r}_{ij}|$. Note that here, each dipole has the same dipole moment, disregarding the influence that other dipoles can have on the magnitude and direction of each of them, an effect that is incorporated in the cdm through the second term on the right of Eq. (5). The anisotropy factor is given by

$$f_\parallel^{ddm} - f_\perp^{ddm} = -2\frac{V^{ddm}(\theta=0) - V^{ddm}(\theta=\pi)}{N\alpha E^2}. \qquad (12)$$

Note that Eq. (11) corresponds to the small-α limit of Eq. (10), since $\boldsymbol{\alpha}_c = N\alpha\mathbf{I} + \alpha^2\mathbf{t} + \mathcal{O}(\alpha^3)$, where $\mathbf{t} = \sum_{i,j}\mathbf{T}_{ij}$ is a 3×3 matrix that depends on the shape of the particle. Within this limit we find that $\mathcal{V}_E(\theta) \approx -\alpha^2(t_\parallel - t_\perp)\cos^2\theta|\mathbf{E}|^2/2$.

From Fig. 2(b) it is clear that for negative α, the anisotropy factor $\left(f_\parallel - f_\perp\right)$ computed with the cdm converges to that of the ddm. We thus find that the decoupled dipole method can be used to approximate the anisotropy factor, yielding accurate results for negative α, at least in the parameter regime of present interest. This is a very useful result, since the computation of anisotropy factors with the ddm is computationally less involved than the equivalent cdm procedure, and is not limited to as narrow a range of polarizabilities as the cdm since it circumvents the polarization catastrophe. Of course the actual accuracy of the ddm for deeply negative polarizabilities is not guaranteed, we just have nothing to compare it to in this regime.

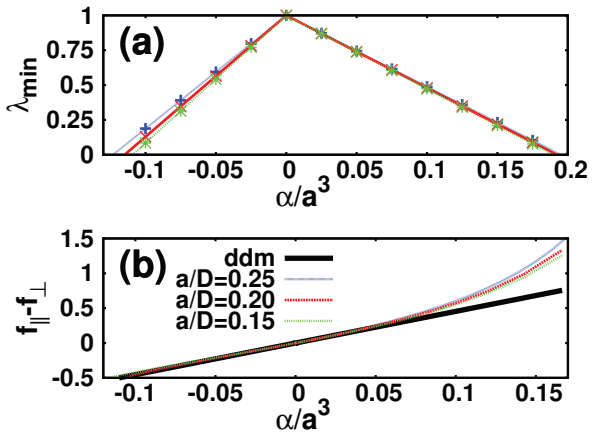

Figure 2. (a) The value of λ_{min}, the smallest eigenvalue of $(\mathcal{I}-\alpha\mathcal{T})$, of a spherocylinder with length-to-diameter ratio $L/D = 2.4$, as a function of the polarizability α, as calculated with the coupled dipole method for different lattice spacings a. The cdm is only applicable if this smallest eigenvalue is larger than zero, corresponding to a range of approximately $-0.12 \lesssim \alpha/a^3 \lesssim 0.19$. (b) Anisotropy factor $\left(f_\parallel - f_\perp\right)$ of the system. The result for the decoupled dipole method (ddm) is also shown (see text).

ORIENTATION DISTRIBUTION

We consider a dilute system of colloidal rods, modeled as spherocylinders with cylinder length L and diameter D, in a dielectric liquid medium exposed to the external electric field $\mathbf{E}$. The excess interaction strength between one spherocylinder and the electric field is given by Eq. (10), and hence the probability distribution $\Psi(\theta)$ of the relative angle $\theta \in [0,\pi/2]$ between a rod and the electric field can be written as the normalized Boltzmann factor

associated with the energy $\mathcal{V}_E(\theta)$, which is given by [37]

$$\Psi(\theta) = \frac{e^{-\beta \mathcal{V}_E(\theta)}}{\int_0^{\pi/2} d\theta \sin\theta e^{-\beta \mathcal{V}_E(\theta)}}, \quad (13)$$

where $\beta^{-1} = k_B T$ with T the temperature and k_B the Boltzmann factor.

We introduce the order parameter

$$S = \int_0^{\pi/2} d\theta \sin\theta \Psi(\theta) \frac{3\cos^2\theta - 1}{2}, \quad (14)$$

which is a quantitative measure of the field-induced nematic ordering of the rods, yielding $S = 1$ for perfect alignment and $S = 0$ for an isotropic angular distribution function.

Although the distribution $\Psi(\theta)$ and the order parameter S are natural quantities to consider from a theoretical perspective, they are not necessarily the most convenient measurable quantities. Below we will present confocal microscopy measurements in which slices of 3D samples are imaged, showing only projections of rods onto the confocal imaging plane. In order to bridge the gap between theoretical and experimentally accessible quantities, we now calculate the projected 2D orientation distribution function $\Psi_{2D}(\theta')$ and the associated nematic order parameter S_{2D} from our fully 3D theoretical predictions as follows. In a single confocal microscopy image the angle θ' between the electric-field direction $\hat{\mathbf{e}}$ and the projected particle orientation vector $\mathbf{w}'$ is measured, rather than the polar angle $\theta = \arccos(\hat{\mathbf{w}} \cdot \hat{\mathbf{e}})$ between the electric field and the actual orientation of the rod $\hat{\mathbf{w}}$, see Fig. 3. Here the projected orientation vector is defined as $\mathbf{w}' \equiv \hat{\mathbf{w}} - (\hat{\mathbf{w}} \cdot \hat{\mathbf{n}})\hat{\mathbf{n}}$, where $\hat{\mathbf{n}}$ denotes the normal of the focal plane. Note that $\mathbf{w}'$ is *not* a unit vector. In our experiments the focal plane is chosen such that $\hat{\mathbf{n}} \perp \hat{\mathbf{e}}$, see Fig. 3. Elementary geometry relates the polar angle θ and the azimuthal angle ϕ of $\hat{\mathbf{w}}$ to the measured angle θ' by

$$|\sin\phi| = \frac{\tan\theta'}{\tan\theta}, \quad (15)$$

where we use the convention that the azimuthal angle satisfies $\hat{\mathbf{w}} \cdot \hat{\mathbf{n}} = \sin\theta\cos\phi$ and $\hat{\mathbf{w}} \cdot \hat{\mathbf{x}} = \sin\theta\sin\phi$ (and hence $\hat{\mathbf{w}} \cdot \hat{\mathbf{e}} = \cos\theta$). Our measurements are also affected by the finite depth Δ of the focal plane (in the direction parallel to $\hat{\mathbf{n}}$). If the size of Δ is of the same order of magnitude as the spatial dimensions of the rods in the experiment, the probability of detecting a rod in the focal plane is orientation dependent, with rods with $\hat{\mathbf{w}} \parallel \hat{\mathbf{n}}$ having relatively large detection probability since their end may "stick" into the focal plane even though their center of mass position is not in the focal plane. It is reasonable to assume that a spherocylindrical rod of cylinder length L, diameter D and orientation $\hat{\mathbf{w}}$ gets detected with a probability that is proportional to $\Delta + D + L(\hat{\mathbf{w}} \cdot \hat{\mathbf{n}})$, corresponding to an effective length interval of the center of mass in which the rod can be detected in the direction perpendicular to the focal plane (note that $D + L(\hat{\mathbf{w}} \cdot \hat{\mathbf{n}})$ is the end-to-end length $L + D$ of the rod projected onto the normal direction). We furthermore assume that the angular distribution is uniaxial about $\mathbf{E}$ such that it is independent of the azimuthal angle ϕ. Using the weight factor $\Delta + D + L\cos\phi\sin\theta$ to account for the orientation-dependence of the probability of detecting a rod of orientation (θ, ϕ), and taking into account the uniaxiality and the geometric relation of Eq. (15), the probability distribution for the projected orientation reads

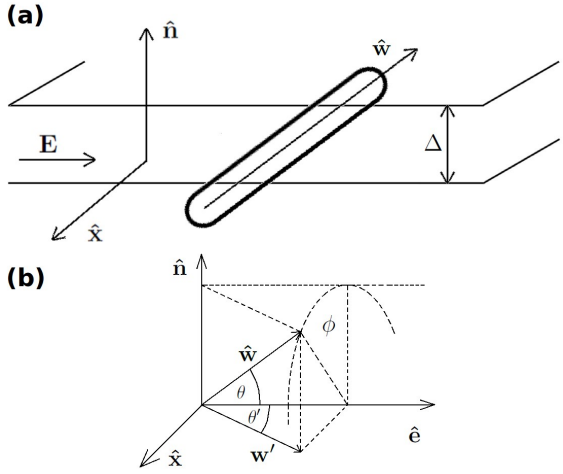

Figure 3. (a) Schematic representation of the rod orientation $\hat{\mathbf{w}}$ with respect to the focal plane of thickness Δ and normal $\hat{\mathbf{n}}$, in the presence of an in-plane electric field $\mathbf{E}$. (b) Schematic representation of the projection $\mathbf{w}'$ of the rod orientation $\hat{\mathbf{w}}$ onto the focal plane. Here, θ denotes the polar angle of $\hat{\mathbf{w}}$ w.r.t. $\hat{\mathbf{e}}$, ϕ the azimuthal angle of $\hat{\mathbf{w}}$, and θ' the angle between $\hat{\mathbf{e}}$ and $\mathbf{w}'$. Here, we choose the coordinate system such that the $\hat{\mathbf{x}}$-direction is perpendicular to $\hat{\mathbf{n}}$ and $\hat{\mathbf{e}}$, with the unit vector $\hat{\mathbf{e}} \parallel \mathbf{E}$.

$$\Psi_{2D}(\theta') = \frac{\int_0^{\pi/2} d\theta \sin\theta \int_0^{\pi/2} d\phi \Psi(\theta) (\Delta + D + L\sin\theta\cos\phi)\, \delta(|\sin\phi| - \tan\theta'/\tan\theta)}{\int_0^{\pi/2} d\theta' \int_0^{\pi/2} d\theta \sin\theta \int_0^{\pi/2} d\phi \Psi(\theta) (\Delta + D + L\sin\theta\cos\phi)\, \delta(|\sin\phi| - \tan\theta'/\tan\theta)}, \quad (16)$$

which is normalized such that $\int_0^{\pi/2} d\theta' \Psi_{2D}(\theta') = 1$ is ensured.

The corresponding order parameter of the projected angular distribution is defined by

$$S_{2D} = \int_0^{\pi/2} d\theta' \Psi_{2D}(\theta') \cos(2\theta') \,, \qquad (17)$$

and takes values between 0 (no ordering) and 1 (perfect ordering along $\hat{\mathbf{e}}$). Fig. 4 compares S_{2D} with the three dimensional order parameter S for a variety of dimensionless length-to-effective-plane-thickness ratios $l = L/(D+\Delta)$, revealing that $S_{2D} \approx S$ for all l and $S \in [0,1]$. In other words, measuring the projected order parameter S_{2D} yields a reliable estimate for the standard $3D$ nematic order parameters S, at least for the functional form $\Psi(\theta) \sim \exp\{C\cos^2\theta\}$ that follows from Eq. (10) and (13). Here $C = \beta(\alpha_{c,\parallel} - \alpha_{c,\perp})|\mathbf{E}|^2/2$ uniquely determines S, leaving l as the only remaining dimensionless parameter in the comparison between S_{2D} and S. We wish to remark here that in the experiments on silica rods, which are described below, the length-to-effective-plane thickness ratio l ranges from $[0.9, 1.8]$.

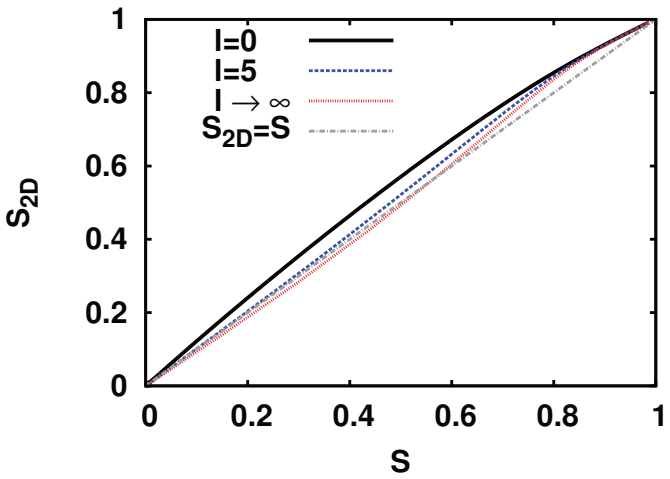

Figure 4. The projected 2-dimensional order parameter S_{2D} as a function of the standard 3-dimensional nematic order parameter S for different values of the length-to-effective-plane-thickness ratio $l = L/(D+\Delta)$. For comparison, we also plot the line $S_{2D} = S$.

EXPERIMENTS

In this section we discuss the colloidal silica rods, and the measurement of their projected orientation distribution functions when exposed to an external electric field. We compare this orientation distribution function to the results of the cdm.

	L/D	L [nm]	D [nm]	Δf^{cdm}	Δf^{ddm}
$B47$	2.4	1480 ± 160	620 ± 40	-0.4444	-0.4572
$B31$	2.7	1730 ± 190	640 ± 50	-0.4621	-0.4753
$N51$	4.0	2130 ± 230	530 ± 30	-0.5126	-0.5280
$B35$	5.0	2750 ± 270	550 ± 60	-0.5366	-0.5533

Table I: Dimensions of rods utilized in the experiments and the corresponding values of $\Delta f = f_\parallel - f_\perp$ as computed with the coupled dipole method for a lattice spacing of $a/D = 0.13$ and the decoupled dipole method for $a/D = 0.05$.

We synthesized four batches of micron-sized silica rods [15, 16]. Systems B35 and B31 consisted of non-fluorescent core particles with a 30 nm FITC-labeled fluorescent inner shell and a 190 nm non-fluorescent outer shell. The rods of B47 had a FITC-labeled core and a 150 nm non-fluorescent shell. Systems N51 had a rhodamine isothiocyanate (RITC) labeled core and a 150 nm non-fluorescent shell. Due to the coated silica layers the particles had approximately the shape of a spherocylinder. We denote by L the length of the cylindrical segment and by D the diameter (values are shown in Table I). The total length of the rods is therefore $L+D$. We prepared dilute dispersions of these rods in a solvent mixture consisting of dimethylsulfoxide (DMSO) with a dielectric constant of 47 and ultrapure water with a dielectric constant of 80. The volume ratio between DMSO and water was 10/0.85 yielding a dielectric constant $\epsilon_2 = 50$ for the medium. The volume fraction of rods in the solvent was about 0.0025, which is a factor 200 below any expected ordering transition and so low that the interactions between rods can safely be ignored [38]. For the sample cells, 0.2×0.2 mm capillaries were used, with two sides coated with gold. A field perpendicular to gravity was created by two 50 μm wires that were connected to the capillary by silverpaint (SPI-paint), with each wire wrapped around a standard electronic wire. For configurations in which several layers of material are positioned between the electrodes, which is the case when the electrodes are on the outside of the capillary, the electric field inside any of these layers can be calculated by:

$$E_i = \frac{V}{\epsilon_i}\left(\frac{\epsilon_1\epsilon_2\epsilon_3}{d_1\epsilon_2\epsilon_3 + d_2\epsilon_1\epsilon_3 + d_3\epsilon_1\epsilon_2}\right), \qquad (18)$$

with V the applied voltage, ϵ_i the dielectric constant of the material the field strength is calculated in, ϵ_{1-3} the dielectric constants of layers $1-3$ and d_{1-3} the thickness of layer $1-3$. In our cells, which consist of two layers of glass ($d = 0.1$ mm, $\epsilon = 3.5$) and one layer of solvent (DMSO/water, $d = 0.1$ mm, $\epsilon = 50$), the field inside the solvent can thus be calculated by $E = 3.4 \cdot 10^{-4} V$ (V/μm). A function generator (Agilent, type 33220A or 33120A) was used to generate a sinusoidal signal with a frequency of 1 MHz and an amplitude of 3.0 V. The generated signal was send to the sample via a wide band am-

plifier (Krohn-Hite, 7602M)), which was used to control the field strength in the sample cell. The field strength was measured by an oscilloscope (Tektronix, TDS3012B or TDS3052). We studied these systems in an external electric field with a confocal microscope (Leica SP2), with the electric field direction $\hat{\mathbf{e}}$ and the normal $\hat{\mathbf{n}}$ of the confocal planes as indicated in Fig. 3, where we estimate $\Delta \approx 1\mu m$. The projected orientation of the rods was determined by analyzing 2D confocal images of rods during sedimentation using an algorithm based on the one described in Ref. [35]. By a counting and binning procedure we measured the projected orientation distribution functions $\Psi_{2D}(\theta')$ for our four different batches of particles, each at several different field strengths. A selection of these results is shown in Fig. 5, revealing (as expected) that the rods can indeed be aligned by field strengths of the order of several tens of V/mm, the more so for stronger fields. In Fig. 5 we also compare these experimental observations with the theoretical predictions that follow from Eqs. (10), (13) and (16), where the parameter $\alpha = -0.281$ nm^3 follows from Eq. (2) with $\epsilon_1 \approx 3.5$ and $n_0 = 19.07$ nm^{-3} (silica), and $\epsilon_2 \approx 50$. The parameters $f_\parallel$ and $f_\perp$, the combination of which is given in Table I, follow accurately from applying the coupled dipole method, in particular Eq. (9), for N equal to several hundred to a thousand dipoles on a cubic lattice filling up spherocylindrical shapes with cylinder length L and diameter D [8, 9]. Note that the value of α is close to the polarization catastrophe, prohibiting us from using very small lattice spacings when applying the cdm. To test our results for the anisotropy factors as calculated with the cdm for $a/D = 0.13$, we compare them with the results obtained with the ddm for $a/D = 0.05$, see Table I. Both sets of results agree well, with a relative difference of about three percent between them. Note that $f_\parallel - f_\perp$ increases monotonically with increasing aspect ratio L/D as expected. Using $f_\parallel - f_\perp$, we calculate the orientation distribution function and the projected nematic order parameter. We see in Fig. 5 that the agreement between the orientation distribution function as measured in the experiments and computed theoretically is reasonable, where one should realize that no fit parameter is involved.

In Fig. 6 we compare the theoretical prediction for S_{2D} with the experimental value

$$S_{2D}^{exp} = \frac{1}{M}\sum_{i=1}^{M}\cos\left(2\theta_i'\right), \qquad (19)$$

as obtained in the experiments for different kinds of rods as a function of the field strength $E = |\mathbf{E}|$. Here, M denotes the total number of rods detected (typically $M \sim 100$) and θ_i' the measured angle of rod i with respect to the electric field direction in the two dimensional measurement plane, see Fig. 3. We see from Fig. 6 that the E-dependence of S_{2D} is quite strong, with S_{2D} varying from 0 for $\sqrt{v_0}E \lesssim 5 \cdot 10^{-6}$ Vm$^{1/2}$ up to $S_{2D} \approx 1$ at $\sqrt{v_0}E \gtrsim 20 \cdot 10^{-6}$ Vm$^{1/2}$, where v_0 denotes the volume of the rod. The combination $\sqrt{v_0}E$ is useful since $\mathcal{V}_E$ scales linearly with v_0 and E^2, and by using this combination on the axis of our graphs the effects of the anisotropy factors can be readily compared for the four different batches of rods, see Eq. (10). The errorbars in Fig. 6 denote standard deviations that stem from the size polydispersity of the rods. Despite some systematic trends that will be discussed in more detail below, a 95% confidence interval of two standard deviations reveals good consistency between experiment and theory for the longer rods in (a) and (b) and to some degree also for the shorter rods of (c), but somewhat less so for the low-field regime of the shortest rods in (d). A possible source of systematic error stems from the image processing routines that were used to analyze the experimental images of the confocal microscope [34]; the measurement of the exact orientation of the rods becomes more and more difficult with decreasing aspect ratio L/D, leading to a possible source of systematic errors that is expected to be most severe for the shortest aspect ratio of L/D = 2.4 [35]. Even though we did not synthesize a sufficiently large number of batches to make a definite statement about this effect we do note that, indeed, the agreement between theory and experiment is best for the longest and worst for the shortest rods. Sample $N51$ (with $L/D = 4$) stands out in the sense that the alignment of the rods with the field as observed in experiments was less or equal than our theory predicts over the whole range of field values sampled, while for the other three samples a systematically stronger alignment was observed in the experiments for intermediate (but not high) field strengths. Interestingly, there is indeed a difference between sample N51 and the other samples, since sample N51 is the only one that contains the dye RITC instead of FITC. Since the dyes are located throughout the rod, this may affect the molecular polarizability α and thereby also the cluster polarizability, which scales with the volume v_0 of the rod. However, since the dye fraction in the rods is only of the order of 10^{-3}, this is most probably not the explanation of this anomalous behavior of sample N51. Another possible explanation for the observation that the alignment of the colloids in the field direction tends to be weaker in the theoretical prediction than in the experiments for intermediate field strengths for all but one set of rods ($N51$), might be that the dimensions of $N51$ could have been overestimated compared to the other three batches

of rods, although we cannot offer an explanation as to why this could have been the case.

We conclude that our theoretical approach yields results that are in good agreement with the measured data for all but the shortest rods as was demonstrated by the favorable comparisons of $\Psi_{2D}(\theta')$ and S_{2D} with the experimentally measured values.

SUMMARY AND OUTLOOK

We succeeded in employing the coupled dipole method to calculate the orientation-dependent excess interaction strength between polarizable colloidal rods and an external electric field. We showed that a decoupled dipole method can be used to circumvent the polarization catastrophe for large negative values of the polarizability. We proceeded to derive the projected orientation distribution function of rods in a focal plane of finite thickness using simple geometric considerations, and found that the measurable projected nematic order parameter S_{2D} is a good estimate for the full $3D$ nematic order parameter S for all $S \in [0, 1]$ and for all rod lengths L, rod diameters D and confocal resolutions Δ. We also synthesized four batches of colloidal silica rods, all with different aspect ratio, and used confocal microscopy to measure the projected orientation distribution and the associated order parameter of very dilute samples in electric fields. Our theoretical predictions without any free fit parameter for the projected orientation distribution and corresponding nematic order parameter are in agreement with the experimental results, the agreement being within a 95% confidence interval for the longest rods and with systematic deviations that probably stem from a limited orientation measurement for the shortest rods. We conclude that our approach to the coupled dipole method in the presence of a solvent can be used to calculate the ordering of dielectric particles of other shapes in an electric field.

ACKNOWLEDGEMENT

This work is part of the research programme of the Foundation for Fundamental Research on Matter (FOM), which is part of the Netherlands Organisation for Scientific Research (NWO). This work is also part of the Delta-ITP consortium, a program of the Netherlands Organisation for Scientific Research (NWO) that is funded by the Dutch Ministry of Education, Culture and Science (OCW).

[1] J.D. Jackson: *Classical Electrodynamics* , 3rd ed. (John Wiley & Sons, Inc., 1999).

[2] A. van Blaaderen, M. Dijkstra , R. van Roij, A. Imhof, M. Kamp, B.W. Kwaadgras, T. Vissers, and B. Liu, European Physical Journal Special Topics **222**, 2895 (2013).

[3] A.-P. Hynninen and M. Dijkstra, Phys. Rev. E **72**, 051402 (2005).

[4] A.-P. Hynninen and M. Dijkstra, Phys. Rev. Lett. **94**, 138303 (2005).

[5] M. Mittal and E.M. Furst, Advanced Functional Materials **19**, 3271 (2009).

[6] E. Kruegel, *The Physics of Interstellar Dust* , (Taylor & Francis Group, 2003).

[7] J.P. Singh, P.P. Lele, F. Nettesheim, N.J. Wagner, and E.M. Furst, Phys. Rev. E **79**, 050401 (2009).

[8] B. W. Kwaadgras, M. Verdult, M. Dijkstra and R. van Roij, J. Chem. Phys. **135**, 134105 (2011).

[9] B. W. Kwaadgras, M. Dijkstra and R. van Roij, J. Chem. Phys. **136**, 131102 (2014).

[10] D. Nagao, M. Sugimoto, A. Okada, H. Ishii, M. Konno, A. Imhof, and A. van Blaaderen, Langmuir **28**, 6546 (2012).

[11] A. F. Demirörs, P. M. Johnson, C. M. van Kats, A. van Blaaderen, and A. Imhof, Langmuir **26** (18), 14466 (2010).

[12] B. Chomiskey, J. D. Albert, H. Yoshizawa and J. Jacobson, Nature **394**, 253, (1998).

[13] H. Kawamoto, Proceedings of the IEEE **90**, 460-500 (2002).

[14] L. Rossi, S. Sacanna and K. P. Velikov, Soft Matter **7**, 64 (2011).

[15] A. Kuijk, A. van Blaaderen, and A. Imhof, J. of the American Chem. Society **133**, 2346 (2011).

[16] A. Kuijk, D. V. Byelov, A. V. Petukhov, A. van Blaaderen, and A. Imhof, Faraday Discussions **159**, 181 (2012).

[17] P.M. Johnson, C.M. van Kats, and A. van Blaaderen, Langmuir **21**, 11510 (2005).

[18] D. Nagao, M. Hashimoto, K. Hayasaka, and M. Konno, Macromol. Rapid Commun. **29**, 1484 (2008).

[19] B. Peng, H. R. Vutukuri, A. van Blaaderen, and A. Imhof, J. Mater. Chem. **22**, 21893-21900 (2012).

[20] H. R. Sheu, M. S. El-Aasser, and J. W. Vanderhoff, J. Polym. Sci. A: Polym. Chem. **28**, 629-651 (1990).

[21] J.-W. Kim, R. L. Larsen, and D. A. Weitz, J. Am. Chem. Soc. **128**, 14374 (2006).

[22] E. B. Mock, H. De Bruyn, B. S. Hawkett, R. G. Gilbert, and C. F. Zukoski, Langmuir **22**, 4037 (2006).

[23] J.-G. Park, J. D. Forster, and E. R. Dufresne, J. Am. Chem. Soc. **132**, 5960 (2010).

[24] M. Yake, R. A. Panella, C. E. Snyder, and D. Velegol, Langmuir **22**, 9135 (2006).

[25] M. Marechal, R. J. Kortschot, A. F. Demirörs, A. Imhof, and M. Dijkstra, Nano Letters **10**, 1907 (2010).

[26] I. D. Hosein and C. M. Liddell, Langmuir **23**, 8810 (2007).

[27] C. I. Zoldesi, C. A. van Walree, and A. Imhof, Langmuir **22**, 4343 (2006).
[28] Z. Cheng, F. Luo, Z. Zhang, and Y.-Q. Ma, Soft Matter **9**, 11392 (2013).
[29] M. Okubo, Y. Konishi, M. Takebe, and H. Minami, Colloid. Polym. Sci. **278**, 919 (2000).
[30] Q. Yang, J. Chen, L. Wang, Q. Xu, and L. He, J. Colloid Interface Sci. **358**, 437 (2011).
[31] S. Sacanna, W. T. M. Irvine, P. M. Chaikin, and D. J. Pine, Nature **464**, 575, (2010).
[32] H.-Y. Kim, J. Sofo, D. Velegol, M. Cole, and A. Lucas, Langmuir **23**, 1735 (2006).
[33] B. W. Kwaadgras, M. Verdult, R. van Roij and M. Dijkstra, J. Chem. Phys. **140**, 154901 (2014).
[34] : M. C. Jenkins and S. U. Egelhaaf, Adv. Colloid. Interf. Sc. **136**, 65 (2008).
[35] T. H. Besseling, M. Hermes, A. Kuijk, B. de Nijs, T.-S. Deng, M. Dijkstra, A. Imhof, and A. van Blaaderen, J. Phys.: Cond. Matter **27**, 194109 (2015).
[36] J. Venermo, A. Sihvola, J. of Electrostatics **63** (2), 101 (2005).
[37] R. van Roij, Eur. J. Phys. **26** S57 (2005).
[38] P.G. Bolhuis and D. Frenkel, J. Chem. Phys. **106**, 666 (1997).

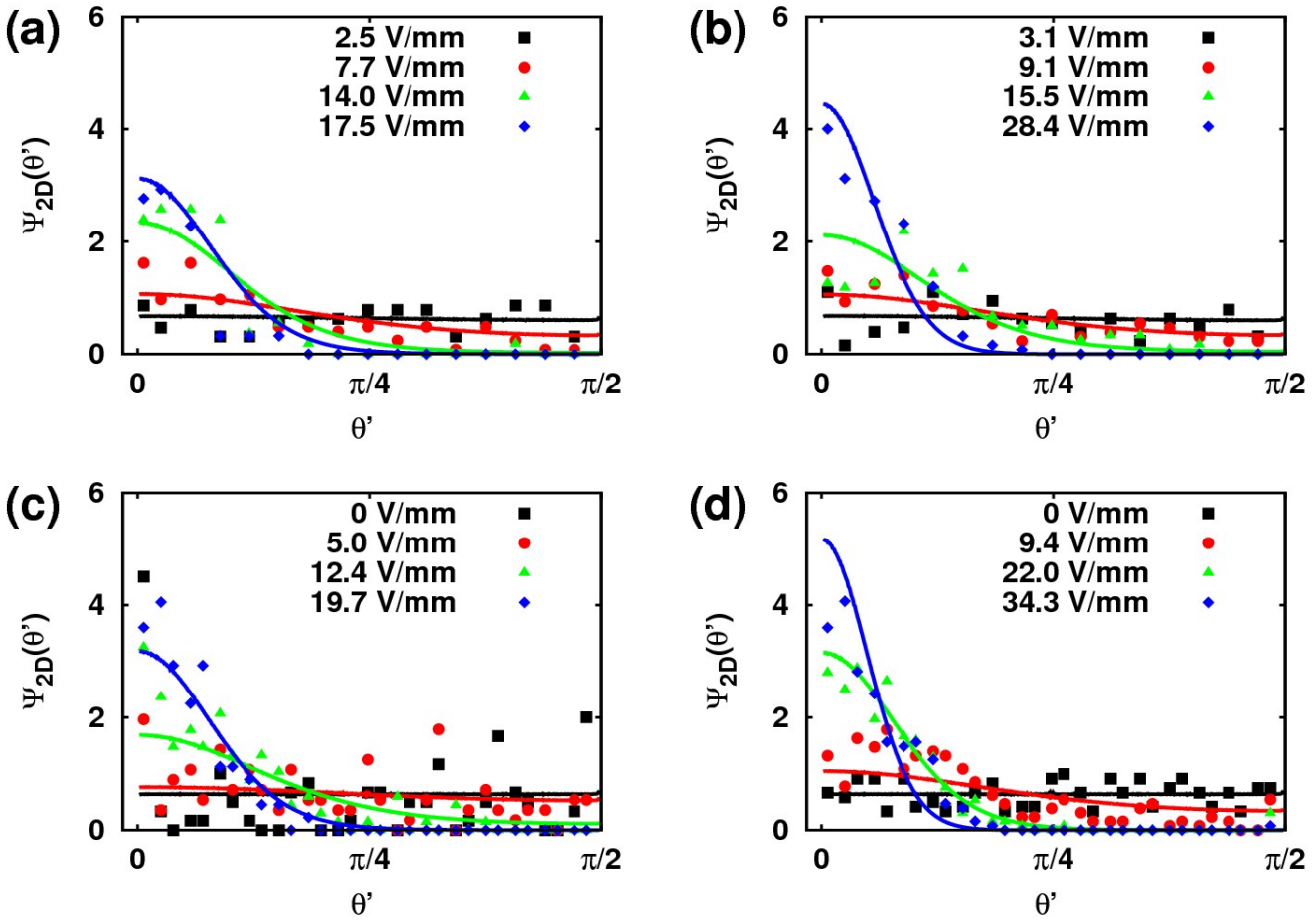

Figure 5. The projected orientation distribution function $\Psi_{2D}(\theta')$ as measured and calculated for the different types of rods, (a) B35 ($L/D = 5$), (b) N51 ($L/D = 4$), (c) B31 ($L/D = 2.7$), (d) B47 ($L/D = 2.4$). Our experimental results are denoted by symbols, our theoretical predictions by lines. Note that no fit parameter was used.

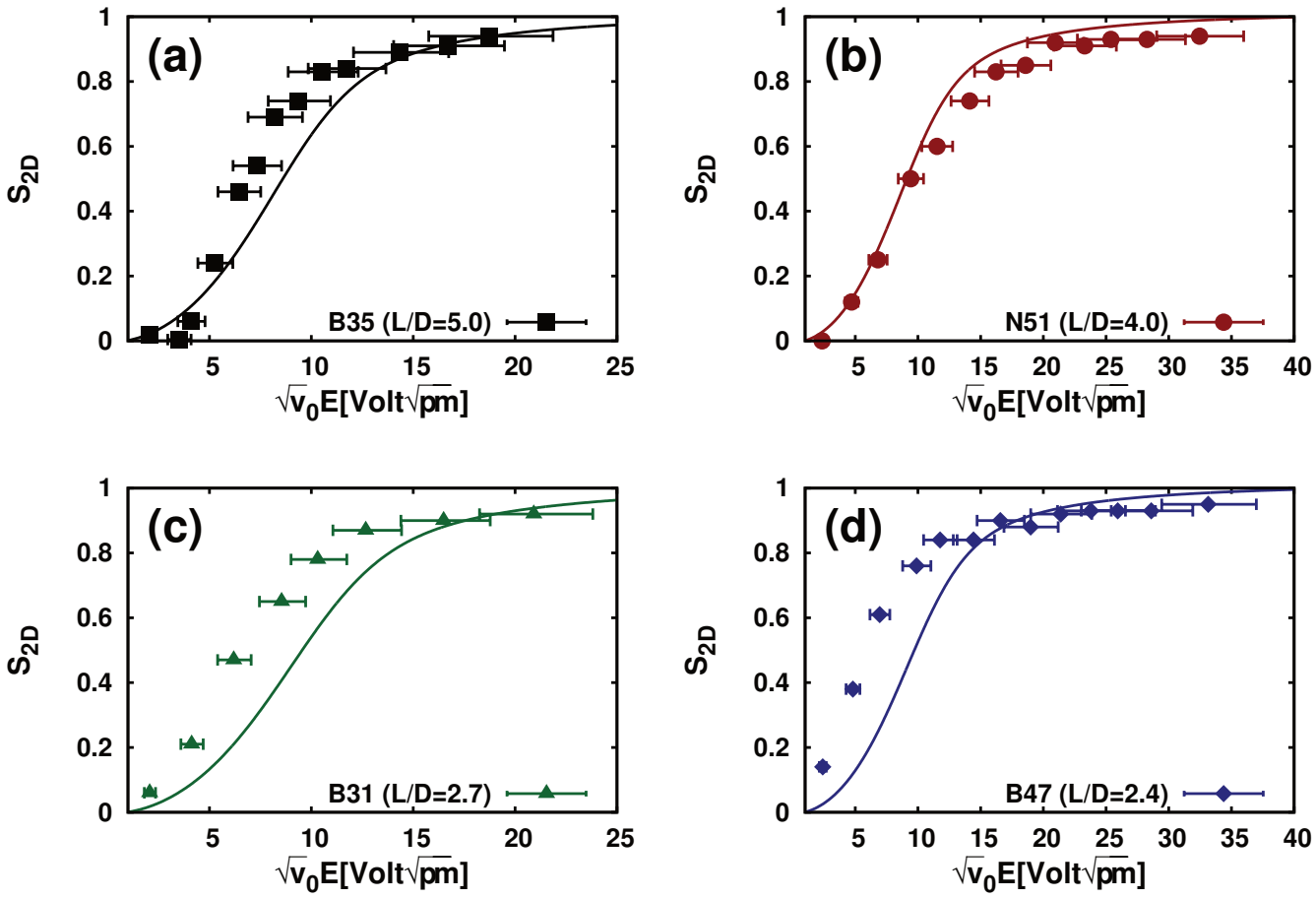

Figure 6. The 2D nematic order parameter S_{2D} as a function of the applied field strength times square root of the particle volume for all four samples of rods as measured (symbols) and calculated from the presently developed theory (curves). The error bars display the results covered within the range of size polydispersity of the rods as denoted in Table I. (a) B35 ($L/D = 5$), (b) N51 ($L/D = 4$), (c) B31 ($L/D = 2.7$), (d) B47 ($L/D = 2.4$).